Published in final edited form as:
Nat Methods. 2019 June 07; 16(8): 711–714. doi:10.1038/s41592-019-0472-1.

Quantitative analysis of super-resolved structures using ASAP

John S. H. Danial[1,2,*] **Ana-J. Garcia-Saez**[1,2]

[1]Interfaculty Institute of Biochemistry, University of Tübingen, Hoppe-Seyler-Straße 4, 72076 Tübingen, Germany

[2]Max Planck Institute for Intelligent Systems, Heisenbergstraße 3, 70569 Stuttgart, Germany

Abstract

Super resolution microscopy allows imaging of cellular structures with high throughput and detail. However, tools for the efficient and quantitative analysis of images generated are lacking. Here, we developed ASAP (Automated Structures Analysis Program) to enable rapid and automated detection, classification and quantification of super-resolved structures. We validate ASAP on ground truth data and demonstrate its broad applicability by analyzing images of nucleoporins, TORC1 complexes, endocytic vesicles and Bax pores.

Recent developments in super resolution microscopy have allowed unprecedented insight into the supramolecular organization of cellular machineries in their native environments[1–7]. Despite those developments, high-throughput innovations in optical nanoscopy[8–11] have, thus far, been unmatched with the demand for rapid and robust analytical tools. The segmentation, analysis and classification of super-resolved subcellular assemblies is heavily prone to human cognitive biases and is still reliant on the use of semi-automated expensive image analysis software packages or non-standard custom-written protocols. Determining the architecture of nanoscopic structures in the cell using available methods can be expensive, time consuming and irreproducible, thereby hindering statistical inference across scales and the understanding of biological function at the molecular level.

To address this limitation, we developed ASAP (Automated Structures Analysis Program), a generic, simple and freely available tool that enables rapid and objective detection, classification and analysis of the macromolecular architecture of cellular assemblies in

Corresponding authors: ana.garcia@uni-tuebingen.de and js2494@cam.ac.uk.
*Present address: Department of Chemistry, University of Cambridge, Lensfield Road, Cambridge CB2 1EW, United Kingdom.

Author contributions
J.S.H.D and A.J.G.S conceived and designed the study, J.S.H.D wrote the software and performed analysis. J.S.H.D and A.J.G.S assessed performance and wrote the manuscript.

Competing financial interests
The authors declare no competing financial interests.

Data Availability Statement
The data that support the findings of this study are available from the corresponding authors upon request.

Code Availability Statement
Source code for ASAP can be obtained from https://github.com/jdanial/ASAP. Compliations of ASAP for Windows and MacOS are available as **supplementary software**.

Europe PMC Funders Author Manuscripts

nanoscopy images. ASAP is provided with a user-friendly graphical interface (Figure 1A). A scripted version that allows pipelining of the analysis workflow for full automation and faster analysis is also included.

ASAP follows a generic approach to the analysis of nanoscopic structures (Figure 1B). It identifies structures using connectivity-based clustering for small and connected structures, or density-based clustering for large and fragmented structures. Accelerated by CPU- and GPU-based parallel computing, ASAP analyzes geometrically the segmented structures to extract relevant shape descriptors. The varied topology of the potential structures of interest and strong behavioral biases involved in describing the extracted topologies has inspired us to deploy a generic machine-learning approach for the automated classification of the analyzed structures. The user starts by training a classifier through annotation of a subset of the structures. The classifier learns to recognize the shape of a structure based on its descriptors. The accuracy of the training process can be improved by annotating more structures, changing the descriptors used for training or selecting a different type of classifier. Once the user is satisfied with the accuracy of the classifier, a classification model can be exported and subsequently used to automatically classify the rest of structures. The classified structures can be revised manually or using semi-automated re-assignment based on values imposed to shape descriptors. Using cluster analysis, ASAP can then group the analyzed structures into distinct populations based on statistical differences in their shape descriptors to help users answer important biological questions related to quantifying assembly states, detecting uneven spatial distributions or analyzing co-recruitment. All generated data can be plotted, modeled, montaged and exported for further analysis, dissemination and reproduction.

ASAP was first tested on ground truth data of exemplary ring structures (Figure 2A). We simulated super-resolved images of 30 nm to 60 nm rings constituted of 8 subunits or epitopes labeled at 50% and 75% efficiencies and sampled with 10 nm and 20 nm precisions. A number of other conditions were also assigned to mimic localization-based imaging experiments (Figure 2A). The simulated structures were input to ASAP, segmented by density, analyzed geometrically and a small subset (146 structures) was used to train the classifier on recognizing rings from fragments (Supplementary note 1). More than 500,000 structures were subsequently segmented, analyzed and classified automatically with ASAP. Rings were selected for further analysis and their radial profiles were fitted to Gaussian functions to extract their radii (Supplementary note 1). We obtained median differential radii ranging from 0.7 nm to 3.3 nm depending on actual radius, labeling efficiency and spatial precision (Figures 2B and C). These remarkable values were obtained for low labeling efficiencies (50 or 75%), large pixel size (10 or 20 nm) and small training volume (146 structures) considering current experimental standards in super-resolution imaging. To test for ASAP robustness against user input, we made systematic changes to the segmentation parameters and measured the radii of the extracted rings (Supplementary note 1). Despite the magnitude of the induced variations (> 20% of the average size of the structures and > 30% of their average intensity), differences between the median absolute differential radii measured for each set of parameters were remarkably low (< 5 Å) (Figure 2D).

We subsequently evaluated the performance of ASAP using super-resolution images of different cellular structures and compared the results with published analysis. Figure 3 shows the results of re-analyzing the architecture of the nuclear pore scaffold published by Szymborska and coworkers12 (Supplementary note 2). Nucleoporins (or Nups) are the main constituting proteins of the nuclear pore complex; a large machinery in the nuclear envelope responsible for the transport of macromolecules between the cell nucleus and cytoplasm13,14. In the published work12, nucleoporin datasets were segmented and analyzed with a combined approach employing strict human-based quality control and electron microscopy image analysis packages. In our analysis, we segmented the structures by density, analyzed them geometrically and used a subset of them to train a classifier (Supplementary note 2). All analyzed structures were automatically classified by ASAP using the classification model previously generated (Figure 3A). We fit the radial profiles of the rings to Gaussian functions to extract the center of their peaks (Supplementary note 2). When comparing the results of the published analysis12 with those generated with ASAP (Figure 3B and C), we obtained a median differential radius of just 4.5 Å corresponding to a root mean squared error (RMSE) of ~9 Å (~1.8% relative to the average radii of the analyzed structures).

We have additionally used ASAP to analyze the nanoscale organization of the protein kinase TORC11 (Supplementary note 3), proteins involved in clathrin-mediated endocytosis15 (Supplementary note 4) and the proapoptotic protein BAX2 (Supplementary note 5) from super resolution microscopy images from previous studies (Supplementary Information). In all cases, we obtained remarkably small deviations (RMSE < 5 nm) between our and published results. This similarity demonstrates the wide applicability of ASAP to a broad range of biological systems at a fraction of the cost and time. In addition, ASAP is entirely image-based and as such, it can process localization-based, coordinate-targeted and computationally-assisted super-resolved images.

There is strong demand for tools that turn super resolution microscopy into a smarter structural biology methodology capable of quantitatively describing single structures in a dynamic biological context. We expect ASAP to fill this important niche and to become a unique and powerful tool enabling full exploitation of the recent developments in high-throughput super resolution imaging9,16,17 for nanoscopy-based structural quantification.

ASAP standalones for Mac OS and Windows, 5 guidance documents and extensive examples are attached as supplementary material.

Supplementary Material

Refer to Web version on PubMed Central for supplementary material.

Acknowledgements

We would like to thank Christian Sieben and Suliana Manley (EPFL) for providing super-resolved images of TORC1, Markus Mund and Jonas Ries (EMBL) for datasets of proteins involved in clathrin-mediated endocytosis and useful discussions, Raquel Salvador-Gallego (University of Colorado Boulder) for helpful discussions on the datasets of the apoptotic protein Bax and Stephanie Alexander and Jan Ellenberg (EMBL) for super-resolved images of nucleoporins. We acknowledge a Max Planck Society (Max-Planck-Gesellschaft) postdoctoral fellowship

awarded to J.S.H.D. This work was supported by Deutsche Forschungsgemeinschaft (DFG) grant GA164/3-1 and the European Research Council (ERC StG – 309966) awarded to A.J.G.S.

References

1. Prouteau M, et al. TORC1 organized in inhibited domains (TOROIDs) regulate TORC1 activity. Nature. 2017; 550:265. [PubMed: 28976958]
2. Salvador-Gallego R, et al. Bax assembly into rings and arcs in apoptotic mitochondria is linked to membrane pores. EMBO J. 2016
3. Bisson-Filho AW, et al. Treadmilling by FtsZ filaments drives peptidoglycan synthesis and bacterial cell division. Science (80-.). 2017; 355:739–743.
4. Betzig E, et al. Imaging Intracellular Fluorescent Proteins at Nanometer Resolution. Sci. 2006; 313:1642–1645.
5. Zhao ZW, et al. Spatial organization of RNA polymerase II inside a mammalian cell nucleus revealed by reflected light-sheet superresolution microscopy. Proc Natl Acad Sci U S A. 2013; 111:681–686. [PubMed: 24379392]
6. Chojnacki J, et al. Maturation-Dependent HIV-1 Surface Protein Redistribution Revealed by Fluorescence Nanoscopy. Science. 2012; 338:524–528. [PubMed: 23112332]
7. Jans D, et al. STED super-resolution microscopy reveals an array of MINOS clusters along human mitochondria. Proc Natl Acad Sci. 2013; 110:8936–8941. [PubMed: 23676277]
8. Holden SJ, et al. High throughput 3D super-resolution microscopy reveals *Caulobacter crescentus* in vivo Z-ring organization. Proc Natl Acad Sci. 2014; 111:4566 LP–4571. [PubMed: 24616530]
9. Gustafsson N, et al. Fast live-cell conventional fluorophore nanoscopy with ImageJ through super-resolution radial fluctuations. Nat Commun. 2016; 7
10. Chen B-C, et al. Lattice light-sheet microscopy: Imaging molecules to embryos at high spatiotemporal resolution. Sci. 2014; 346
11. Almada P, et al. Automating multimodal microscopy with NanoJ-Fluidics. Nat Commun. 2019; 10
12. Szymborska A, et al. Nuclear pore scaffold structure analyzed by super-resolution microscopy and particle averaging. Science. 2013; 341:655–8. [PubMed: 23845946]
13. Grossman E, Medalia O, Zwerger M. Functional Architecture of the Nuclear Pore Complex. Annu Rev Biophys. 2012; 41:557–584. [PubMed: 22577827]
14. Beck M, Hurt E. The nuclear pore complex: understanding its function through structural insight. Nat Rev Mol Cell Biol. 2016; 18:73. [PubMed: 27999437]
15. Mund M, et al. Systematic Nanoscale Analysis of Endocytosis Links Efficient Vesicle Formation to Patterned Actin Nucleation. Cell. 2018; 174:884–896.e17. [PubMed: 30057119]
16. Holden SJ, et al. High throughput 3D super-resolution microscopy reveals Caulobacter crescentus in vivo Z-ring organization. Proc Natl Acad Sci. 2014; 111:4566–4571. [PubMed: 24616530]
17. Li D, et al. Extended-resolution structured illumination imaging of endocytic and cytoskeletal dynamics. Science (80-.). 2015; 349

Europe PMC Funders Author Manuscripts

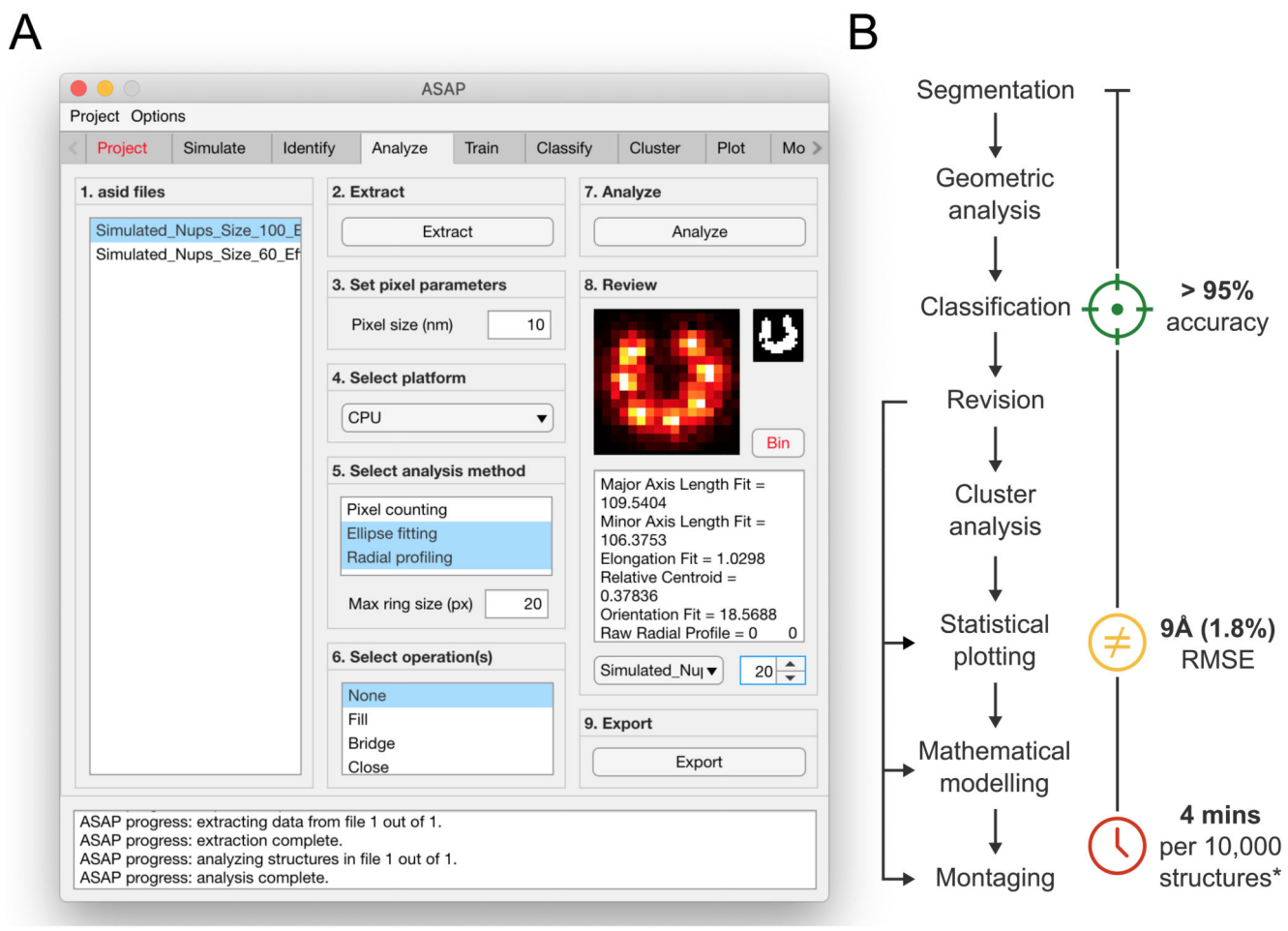

Figure 1. ASAP workflow.

(A) Example window of ASAP graphical user interface. (B) Fully-automated workflow of ASAP along with metrics distinguishing it from other available approaches (*estimate calculated from the analysis of more than 500,000 structures from segmentation to modeling on a laptop with a 1.2 GHz Intel Core M processor and 8 GB of RAM).

Europe PMC Funders Author Manuscripts

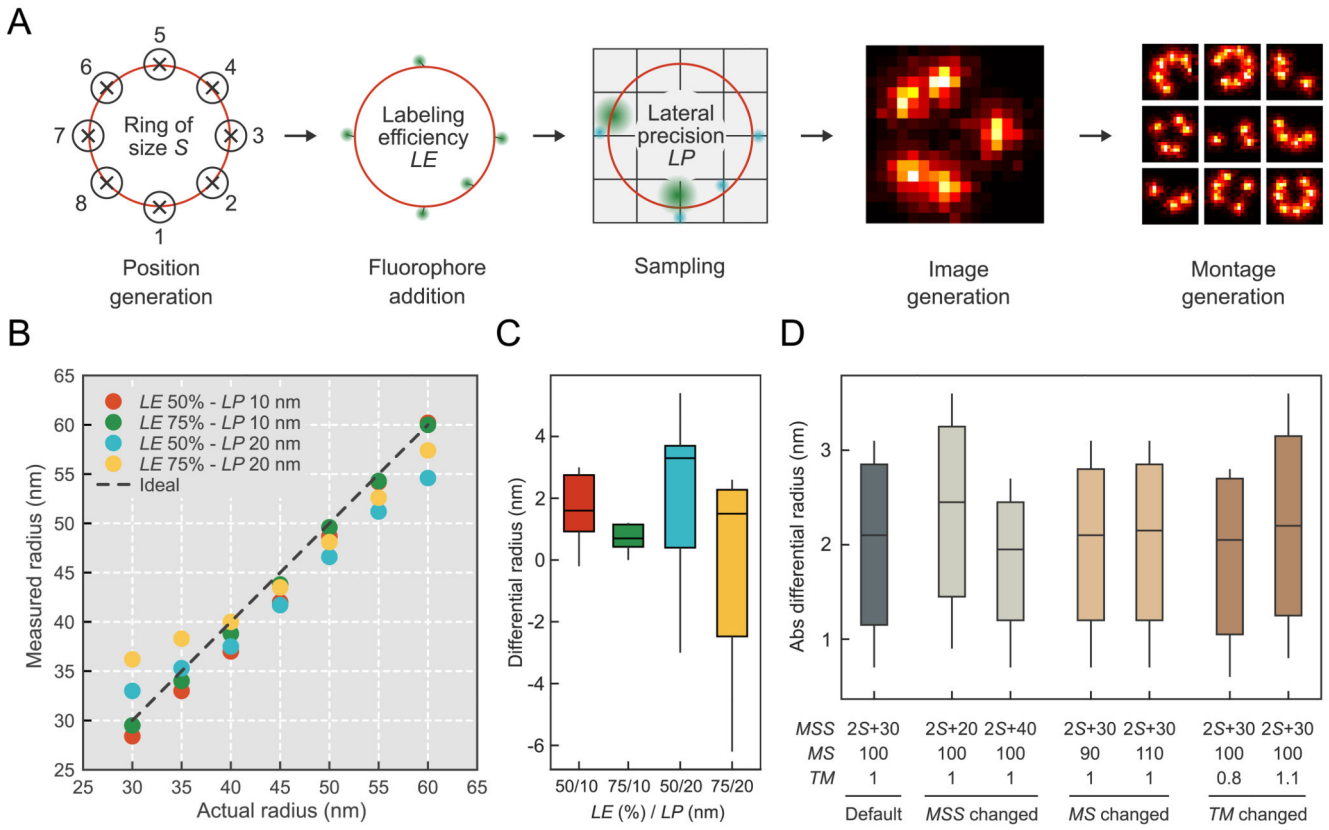

Figure 2. Analysis of simulated structures.

(A) Schematic of the simulation process. We calculated the positions of 8 epitopes comprising a ring of size *S* and added free-to-rotate fluorophores at a labeling efficiency *LE*. Blinking was simulated and sampled with a lateral precision *LP*. *S, LE* and *LP* were respectively set to 30 – 60 nm, 50% & 75% and 10 & 20 nm. Simulated rings were aligned into gapless montages and input to ASAP for analysis following training. Graphs in (B) and (C) show box plots with center lines being medians, box limits being the 25th and 75th percentiles and whiskers comprising all data points within 1.5x the interquartile range. (B) Variation of the measured versus actual radii of the simulated rings under different labeling and sampling conditions. Individual points show the mean measured radii of structures with the same actual radius, labeling efficiency and lateral precision. (C) Difference between actual and measured radii of the simulated rings under different labeling and sampling conditions. The labeling / sampling conditions are: 50% / 10 nm (N = 3343), 75% / 10 nm (N = 9047), 50% / 20 nm (N = 17837) and 75% / 20 nm (N = 24798). (D) ASAP robustness against variations in user input. Absolute differential radius measured as absolute value of the difference between actual and measured radii for 7 different sets of segmentation parameters (from left to right: N = 55025 / N = 63717 / N = 48740 / N = 55954 / N = 54209 / N = 62357 / N = 51189) (*MSS* is Max Structure Size, *MS* is Min Size and *TM* is Threshold Multiplier). Information on selection of ASAP parameters can be found in supplementary guide 2. Exact radii can be found in supplementary note 1.

Europe PMC Funders Author Manuscripts

Europe PMC Funders Author Manuscripts

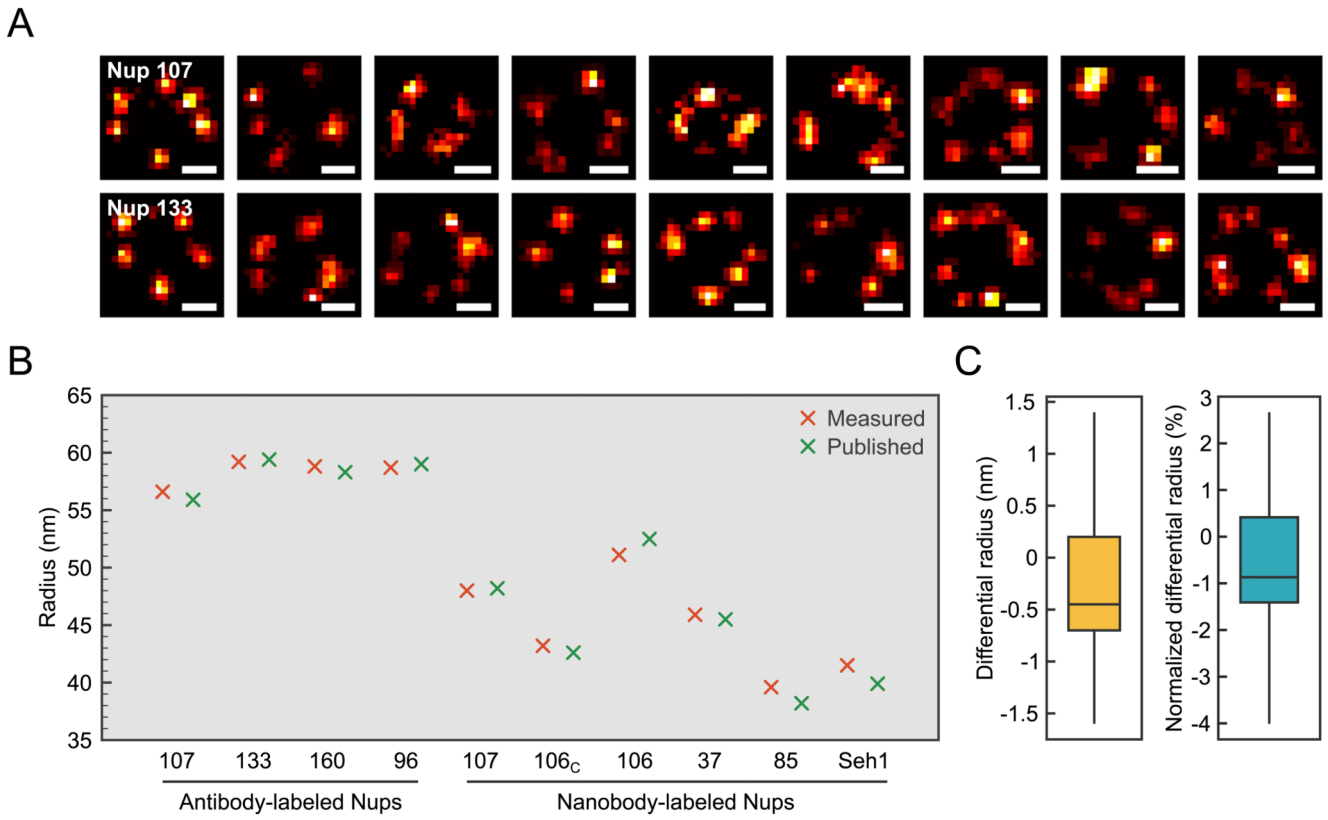

Figure 3. Analysis of super-resolved nucleoporins.

(A) Gallery of a subset of the Nups (Nup107 and Nup133) analyzed with ASAP. Scale bar = 50 nm. (B) Comparison between measured and published radii of the different Nups. (C) Differential radius and normalized differential radius between the published analysis and that of ASAP for all Nups. Graphs show box plots with the center lines being the medians, box limits being the 25th and 75th percentiles and whiskers comprising all data points within 1.5x the interquartile range. Exact radii and counts can be found in supplementary note 2.